Temperature Dependence of the Water Infrared Spectrum: Driving Forces, Isosbestic Points, and Predictions

Zeke A. Piskulich and Ward H. Thompson*

Department of Chemistry, University of Kansas, Lawrence, KS 66045, USA

E-mail: wthompson@ku.edu

Abstract

The temperature derivative of the infrared (IR) spectrum of HOD/D_2O is directly calculated from simulations at a single temperature using a fluctuation theory approach. It is demonstrated, based on an energetic decomposition of the derivative, that the blueshift with increasing temperature is associated with the competition between electrostatic and Lennard-Jones interactions. The same competition gives rise, where their contributions cancel, to a near isosbestic point. The derivative is further used to define an effective internal energy (and entropy) associated with the IR spectrum and it is shown how a van't Hoff relation can be used to accurately predict the spectrum over a wide range of temperatures. These predictions also explain why a precise isosbestic point is not observed.

Graphical TOC Entry

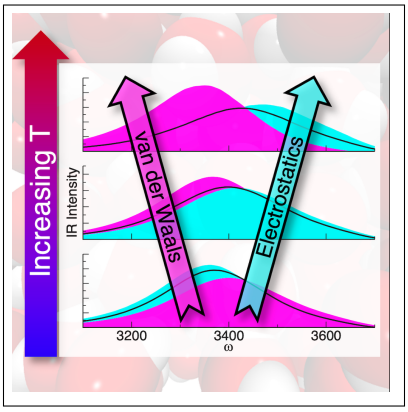

Keywords

vibrational spectroscopy; dynamics; internal energy; entropy; fluctuation theory

The behavior of liquid water vibrational spectra with temperature has long been of interest[1–27] because of the potential insight it can offer into the underlying driving forces for the liquid structure and dynamics. Among the prominent features observed are isosbestic points found in the IR[4,9–11] and Raman[2,6,7,12,13,16–18,26,27] spectra as temperature is varied. These have been used to argue for two-state models of the water hydrogen-bond (H-bond) network,[4,6,8,9,11] but more recently it has been shown they instead arise as a natural feature of inhomogeneous broadening.[16–18]

In this Letter, we investigate the energetic origins of the temperature dependence of the IR spectrum of dilute HOD in D_2O to shed new light on these issues. Specifically, we directly calculate the temperature derivative of the IR spectrum using molecular dynamics (MD) simulations. The theoretical approach is an application of fluctuation theory to dynamics,[28–31] similar to that previously described by Morita and co-workers.[22–25] This method provides new mechanistic insight into the energetic driving forces – *e.g.*, kinetic energy, Coulombic and Lennard-Jones interactions – behind spectral changes with temperature, including the nature and origin of the isosbestic point. We show that the effects can be characterized by an (effective) internal energy as a function of frequency, which itself can be used to predict the IR spectrum for temperatures spanning at least 80 K.

We calculate the IR lineshape from the Fourier transform

$$I(\omega) = \frac{1}{2\pi} \int_{-\infty}^{\infty} e^{-i\omega t}\, \phi(t)\, dt, \tag{1}$$

of the dipole-dipole response function,

$$\phi(t) = \left\langle \vec{\mu}_{01}(0) \cdot \vec{\mu}_{01}(t)\, e^{i \int_0^t \omega_{01}(\tau)\, d\tau} \right\rangle e^{-|t|/2T_1}. \tag{2}$$

Here $\vec{\mu}_{01}(t) = \langle 1|\hat{\mu}|0\rangle = \mu_{01}(t)\, \vec{e}_{OH}(t)$ is the matrix element of the transition dipole moment vector for the OH bond at time t, $\omega_{01}(t)$ is the $0 \rightarrow 1$ vibrational frequency at time t, and T_1 is the $n = 1$ vibrational relaxation lifetime. The brackets $\langle \cdots \rangle$ indicate a thermal average.

It is within this thermal average that the temperature dependence of the IR spectrum appears in two factors: the Boltzmann weighting factor in the average and the canonical partition function that normalizes it.[29,31] Thus, taking the derivative of the IR lineshape gives a simple expression

$$\frac{dI(\omega)}{d\beta} = -\frac{1}{2\pi}\int_{-\infty}^{\infty} e^{-i\omega t}\,\phi_H(t)\,dt, \tag{3}$$

where $\beta = 1/k_BT$ with k_B Boltzmann's constant and $\phi_H(t)$ is, within a sign, the β derivative of $\phi(t)$,

$$\frac{d\phi(t)}{d\beta} = -\left\langle \delta H(0)\,\vec{\mu}_{01}(0)\cdot\vec{\mu}_{01}(t)\,e^{i\int_0^t \omega_{01}(\tau)\,d\tau}\right\rangle e^{-|t|/2T_1} = -\phi_H(t). \tag{4}$$

Here, $\delta H(0) = H(0) - \langle H\rangle$ is the fluctuation in the total system energy from its average value. For simplicity, we neglect the temperature dependence of T_1 and use the value of 700 fs from Fecko *et al.*[32]

In this work, we evaluate these quantities using the empirical mapping approach[15,33,34] from a classical MD simulation of H_2O, considering each OH bond as independent and isotopically dilute (*i.e.*, neglecting vibration-vibration coupling) to effectively model dilute HOD in D_2O.[15] In this approach, ω_{01} and μ_{01} are obtained from the electric field along the OH bond, exerted by the surrounding waters on the H atom of interest, as determined by a correlation with electronic structure results. This approach has been shown to be accurate for a water in a variety of environments[34] and over a wide range of temperatures.[15,35]

The simulated IR lineshape for HOD in D_2O is presented in Fig. 1a. The peak maximum is at 3382 cm^{-1} and the full-width half-maximum (FWHM) is 270 cm^{-1}. It is interesting to compare the IR lineshape with the distribution of frequencies, $P(\omega) = \langle\delta[w - w_{01}(\mathbf{Q})]\rangle$, which is also plotted in Fig. 1a. $P(\omega)$ is notably blueshifted, with a maximum at 3465 cm^{-1}, broader (FWHM = 382 cm^{-1}), and more asymmetric with a long tail to lower frequencies. The differences are partially a result of non-Condon effects, *i.e.*, the transition dipole moment that governs the IR intensity is larger for stronger H-bonds, which are captured in the spectral

density, $P_\mu(\omega) = \langle |\mu_{01}(\mathbf{Q})|^2 \, \delta[w - w_{01}(\mathbf{Q})] \rangle$. The spectral density is also plotted in Fig. 1a and more closely resembles the IR lineshape: it peaks at 3385 cm^{-1} but is still broader (FWHM = 361 cm^{-1}). The difference between the the IR lineshape and spectral density can be attributed primarily to dynamical effects, particularly motional narrowing resulting from rapid fluctuations of the vibrational frequency.[36]

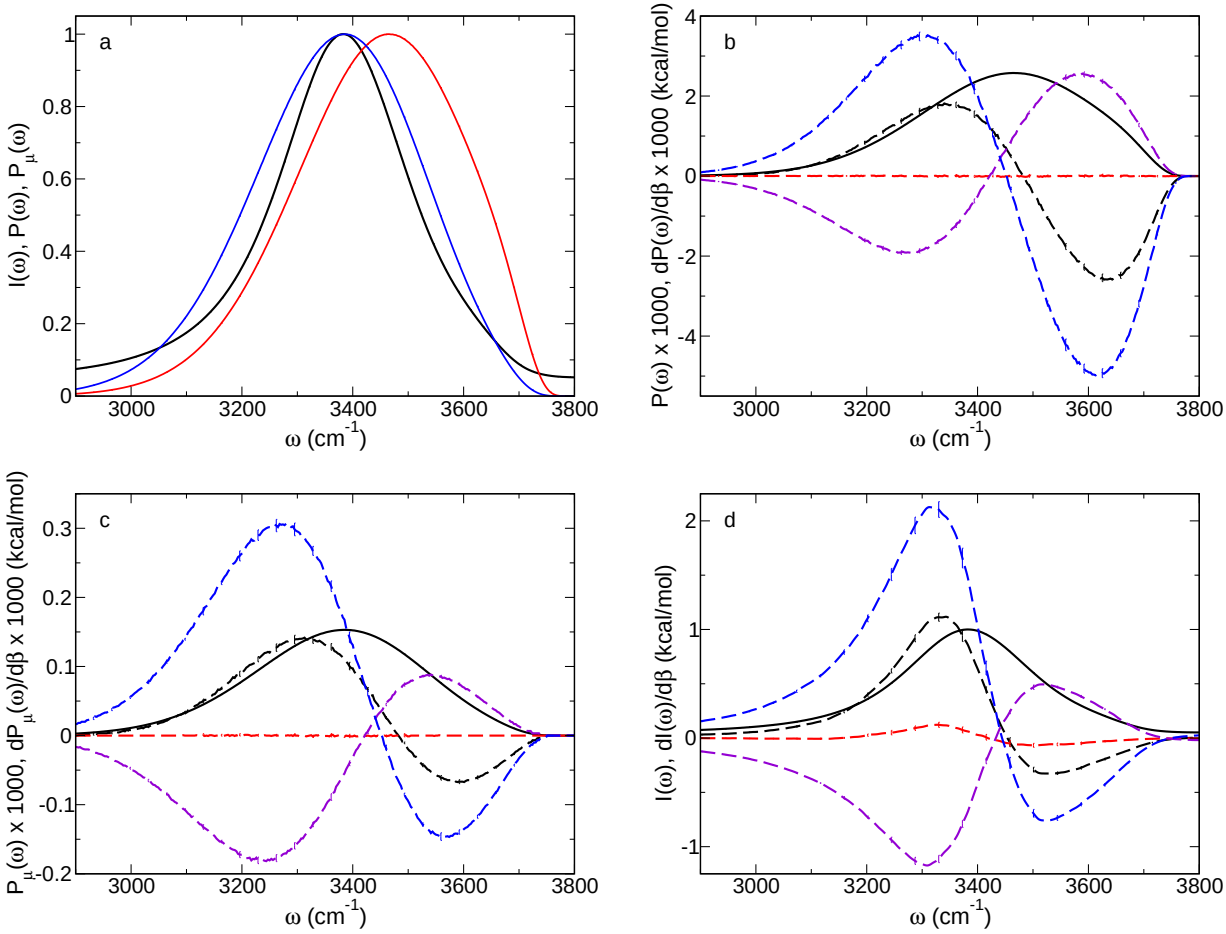

Figure 1: (a) HOD in D_2O IR spectrum (black), frequency distribution (red), and spectral density (blue) at 298.15 K. The (b) frequency distribution, (c) spectral density, and (d) IR spectrum, with the maximum set to 1, are reproduced (solid black) along with the total derivative with respect to β (dashed black) and the contributions to the derivative from the kinetic (dashed red), Lennard-Jones (dashed violet), and Coulombic (dashed blue) energies.

The temperature (or β) derivative of the frequency distribution and spectral density can

be calculated like that for $I(\omega)$,

$$\frac{dP(\omega)}{d\beta} = -\langle \delta H \, \delta[w - w_{01}(\mathbf{Q})] \rangle \equiv -P_H(\omega), \tag{5}$$

and

$$\frac{dP_\mu(\omega)}{d\beta} = -\langle \delta H \, |\mu_{01}|^2 \, \delta[w - w_{01}(\mathbf{Q})] \rangle \equiv -P_{\mu,H}(\omega). \tag{6}$$

A key advantage of this approach is that it provides additional mechanistic information because the system energy is divisible into physically meaningful components, *e.g.*, $\delta H(0) = \delta KE(0) + \delta V_{LJ}(0) + \delta V_{Coul}(0)$, yielding the contributions to the derivative from each of these motions or interactions, *e.g.*, $P_H(\omega) = P_{KE}(\omega) + P_{LJ}(\omega) + P_{Coul}(\omega)$. Here, KE is the kinetic energy and V_{LJ} and V_{Coul} are the Lennard-Jones and Coulombic potential energies. It should be noted that other decomposition are possible as long as the terms sum to the total energy; though for the present work we consider the simple decomposition above. The total temperature derivatives of $P(\omega)$, $P_\mu(\omega)$, and $I(\omega)$ are shown in Fig. 1b-d along with the contributions to each derivative from the different energy components.

Considering the frequency distribution first, Fig. 1b shows that the total derivative is positive at lower frequencies (*i.e.*, the amplitude in this region will grow as β increases and T decreases) and negative at higher frequencies. Note that because $P(\omega)$ is a normalized probability distribution, its derivative must integrate to zero. This gives rise to at least one frequency where the derivative is zero and therefore where $P(\omega)$ is unchanged by temperature (at least over some interval). Geissler has previously pointed this out in the context of understanding isosbestic points that have been observed in the Raman and IR spectra of water,[16–18] the former of which can often be well described by the frequency distribution.

New insight into the origin of the isosbestic point is offered by the energetic contributions to the derivative. Because $P(\omega)$ depends only on configurational variables, the kinetic energy contribution is rigorously zero. The total derivative, $dP(\omega)/d\beta$, is thus determined by the direct competition of the Lennard-Jones and Coulombic interactions. Namely, in an

H-bond the waters sit on the repulsive wall of the Lennard-Jones potential, held there by the attractive Coulombic attraction between the donor H atom and the accepting O atom. The frequency distribution captures a continuum of H-bond structures with lower frequencies corresponding to greater electrostatic stabilization and larger Lennard-Jones repulsion. Conversely, the highest frequencies, which reflect weak or even transiently broken H-bonds, involve more favorable Lennard-Jones and poorer Coulombic interactions. This behavior is reflected in the Lennard-Jones and Coulombic contributions to the $P(\omega)$ derivative shown in Fig. 1b. The former favors higher frequencies and the latter favors lower frequencies as T decreases. The electrostatic interactions are dominant, so the total derivative reflects the partial cancellation of the Coulombic contribution by the Lennard-Jones term.

The frequency where the total derivative is zero, the isosbestic point for $P(w)$ with changes in T, is thus determined by the competition between the Coulombic and Lennard-Jones interactions that are held in tension in an H-bond.[37–39] The same battle between these interactions explains an analogous isosbestic point in the water O–O radial distribution function,[37] which has been observed in both measurements and simulations.[40–43]

The IR spectrum differs from the frequency distribution due to both non-Condon and dynamical effects (Fig. 1a). The effect of the former on the temperature dependence is explored in Fig. 1c, where the spectral density derivative, $dP_\mu(\omega)/d\beta$, is shown along with its kinetic, Lennard-Jones, and Coulombic energy contributions. These are qualitatively similar to those for the frequency distribution. Indeed, the spectral density is the frequency distribution weighted by the average square transition dipole moment at each frequency, increasing the relative amplitude of both $P_\mu(\omega)$ and its derivatives at lower frequencies compared to $P(\omega)$. The temperature dependence of $P_\mu(\omega)$ and $P(\omega)$ thus only differ if $\langle|\mu_{01}|^2\rangle(\omega)$ changes with temperature. Within the empirical mapping description this is not the case and there is no temperature dependence of the non-Condon effect itself.

Because the IR spectrum includes dynamical effects that significantly affect the lineshape, it is perhaps not obvious that it would retain an isosbestic point. This is explored in Fig. 1d,

which shows the total derivative of $I(\omega)$ with respect to β and it energetic components. The total derivative is in general agreement with that previously reported by Joutsuka and Morita using a flexible, polarizable water model to directly describe the frequencies;[25] they did not report energetic decompositions. The results clearly show that the general shape of $dI(\omega)/d\beta$ is similar to that for the frequency distribution and spectral density, including the presence of a frequency at which the derivative is zero, indicative of an (at least local) isosbestic point at 3454 cm^{-1}, which is redshifted relative to the 3482 cm^{-1} found for $P(\omega)$ and $P_\mu(\omega)$; experiments on H_2O find an isosbestic point at 3460 cm^{-1}.[10] As with the frequency distribution, this can be understood based on the energetic contributions to the derivative, which measure how the interactions drive the changes in $I(\omega)$ with T. The dynamical nature of the IR lineshape means that the kinetic energy contribution to its derivative is non-zero, but it remains quite small. Thus, $dI(\omega)/d\beta$ is largely determined by the competition between the Coulombic and Lennard-Jones interactions of the water molecules that, as T is decreased, favor lower and higher OH frequencies, respectively.

It is interesting and useful to examine the thermodynamics that underlie the frequency distribution by considering the corresponding (Helmholtz) free energy profile as a function of frequency,

$$\Delta A(\omega) = -k_B T \ln P(\omega) = \Delta U(\omega) - T\Delta S(\omega), \tag{7}$$

where $\Delta U(\omega)$ and $\Delta S(\omega)$ are the internal energy and entropy. It is straightforward to show that, within the van't Hoffian assumption that $\Delta U(\omega)$ and $\Delta S(\omega)$ are temperature independent,[37]

$$\Delta U(\omega) = \frac{P_H(\omega)}{P(\omega)}. \tag{8}$$

The entropic contribution can be directly obtained from $\Delta A(\omega)$ and $\Delta U(\omega)$. Geissler derived an analogous expression to Eq. 8 in explaining the ubiquity of isosbestic points.[17,18] (The spectral density free energy is the same as that for $P(\omega)$ within the present model.) In addition, because $P_H(\omega)$ can be decomposed into Lennard-Jones and Coulombic contributions,

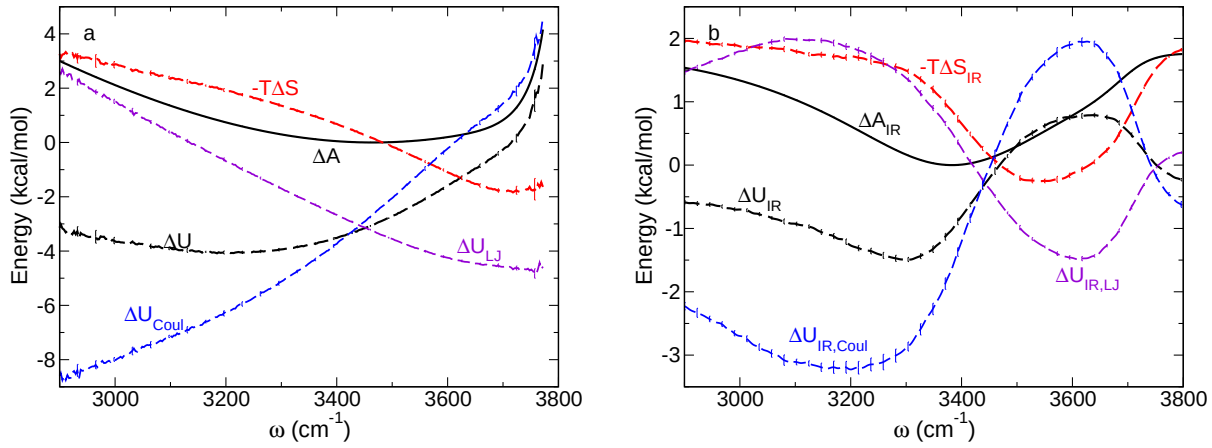

Figure 2: Free energy ΔA (solid black), internal energy ΔU (dashed black), entropic contribution $-T\Delta S$ (dashed red) are plotted versus frequency along with the Lennard-Jones (dashed violet) and Coulombic (dashed blue) internal energy components for the (a) frequency distribution and (b) IR spectrum at 298.15 K.

so can the internal energy. Namely,

$$\Delta U(\omega) = \frac{P_{LJ}(\omega)}{P(\omega)} + \frac{P_{Coul}(\omega)}{P(\omega)} = \Delta U_{LJ}(\omega) + \Delta U_{Coul}(\omega), \tag{9}$$

providing additional insight into the energetic driving forces.

The free energy, internal energy, entropy, and internal energy components for the frequency distribution are shown in Fig. 2a. The internal energy $\Delta U(\omega)$ has a broad minimum around 3200 cm^{-1} resulting from the competition between the Coulombic and Lennard-Jones contributions. The former decreases monotonically toward lower frequencies, *i.e.*, more red-shifted, strongly hydrogen-bonded OH groups, while the latter decreases monotonically as the frequency increases. The entropic contribution, $-T\Delta S(\omega)$, also favors higher frequencies, further indicating that they correspond a more disordered H-bonding arrangement involving weaker, or even transiently broken, H-bonds.

The IR spectrum, as a dynamical quantity, cannot be rigorously converted to a free energy, but we can consider an effective free energy defined in analogy to Eq. 7:

$$\Delta A_{IR}(\omega) = -k_B T \ln I(\omega) = \Delta U_{IR}(\omega) - T\Delta S_{IR}(\omega). \tag{10}$$

Analogous to the frequency distribution, the internal energy can be decomposed as $\Delta U_{IR}(\omega) = \Delta U_{IR,KE}(\omega) + \Delta U_{IR,LJ}(\omega) + \Delta U_{IR,Coul}(\omega)$, noting that the kinetic energy contribution is non-zero.

These effective free energy, internal energy, entropy, and internal energy components for the IR spectrum are shown in Fig. 2b. They exhibit behavior that is generally the same as for the frequency distribution, with the primary difference occurring at the highest and lowest frequencies. Namely, $\Delta A_{IR}(\omega)$ asymptotically approaches constant values at the limits of the spectrum. Similarly, $\Delta U_{IR}(\omega)$ and $-T\Delta S_{IR}(\omega)$ exhibit local maxima and minima due to this behavior. This difference in shapes with the $P(\omega)$ results is due to both non-Condon effects, which appear only in the free energy and entropy since the transition dipole moment is not T dependent, and dynamical effects such as motional narrowing (see Fig. 1a); the latter make these only effective energy curves. Otherwise, the results for the IR spectrum show the same competition between Coulombic and Lennard-Jones interactions as well as between internal energy and entropic factors.

Effective internal energy curves have been previously reported by Hare and Sorenson[6] and Walrafen[13] obtained from numerical derivatives of the water Raman spectrum. They obtained shapes quite similar to the $\Delta U_{IR}(\omega)$ shown in Fig. 2b. They assigned the energy difference between the maximum and minimum in $\Delta U_{IR}(\omega)$ to that required to break an H-bond; here we find that difference to be 2.3 kcal/mol whereas they obtained 3.2 and 5.1 ± 0.5 kcal/mol.[6,13] We have separately calculated the activation energy for an H-bond exchange, or "jump," (see Ref. 39) and find $E_{a,jump} = 3.79 \pm 0.06$ kcal/mol. Thus, the present results are not consistent with such an interpretation, though this may be related to the larger non-Condon effects present in the IR spectrum.

A key advantage of calculating $\Delta U(\omega)$ is that it provides a van't Hoff approach to predict $P(\omega)$ at different temperatures from a single temperature simulation as

$$P_{pred}(\omega; T_b) = \frac{P(\omega; T_a)\, e^{-(\beta_b - \beta_a)\Delta U(\omega)}}{\int P(\omega; T_a)\, e^{-(\beta_b - \beta_a)\Delta U(\omega)}\, d\omega}. \tag{11}$$

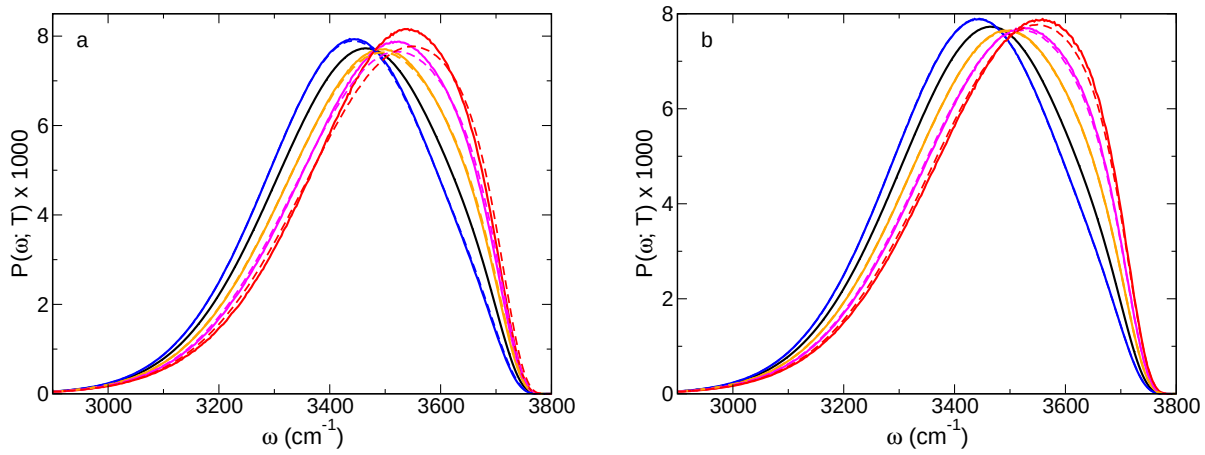

Figure 3: Predicted frequency distribution (solid lines) for 280 (blue), 320 (orange), 340 (magenta), and 360 K (red) from the 298.15 K distribution (black) and its derivative; direct calculations at these temperatures are shown as dashed lines of the same color. Results are shown based on (a) first-order Taylor series approximations and (b) van't Hoff predictions, Eq. 11.

The denominator is included to account for the fact that $\exp\{-(\beta_b-\beta_a)\Delta U(\omega)\}$ is not norm conserving. Here the a and b subscripts label the simulation and predicted temperature, respectively. The frequency distribution at other temperatures predicted from Eq. 11 based on $P(\omega)$ and $\Delta U(\omega)$ calculated at 298.15 K are shown in Fig. 3b and compared to the distributions calculated directly at the same temperatures. The agreement is excellent. Only for the highest temperature, 360 K, are there any significant differences between the predicted and directly calculated distributions, where the predicted distribution is slightly too narrow. These shortcomings of the predictions are indicative of non-van't Hoff behavior, *i.e.*, temperature dependence of $\Delta U(\omega)$ and $\Delta S(\omega)$.

The directly calculated and predicted frequency distributions do not exhibit a precise isosbestic point, but only an approximate one, which is a consequence of the normalizing denominator in Eq. 11. Without it, the frequency distribution would have a rigorous isosbestic point at the frequency where $\Delta U(\omega) = 0$, *i.e.*, where $dP(\omega)/d\beta = 0$. Note that a first-order Taylor series expansion of the exponential in Eq. 11, $P_{1st-order}(\omega; T_b) = P(\omega; T_a)\,[1-(\beta_b-\beta_a)\Delta U(\omega)]$, does conserve the normalization of the distribution, illustrating the local nature of the isos-

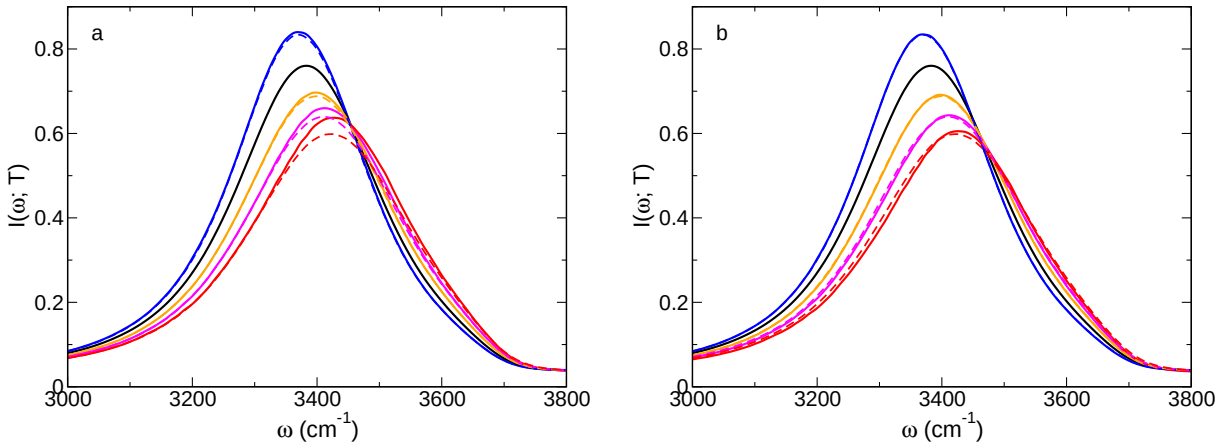

Figure 4: Predicted IR spectrum (solid lines) for 280 (blue), 320 (orange), 340 (magenta), and 360 K (red) from the 298.15 K spectrum (black) and its derivative; direct calculations at these temperatures are shown as dashed lines of the same color. Both (a) unnormalized and (b) normalized results, Eq. 12, are shown (see the text).

bestic point. Results from this description are shown in Fig. 3a. The approximation is reasonable for approximately ±20 K from the temperature at which the derivative is calculated, but leads to significant deviations for larger variations in the temperature.

The temperature dependence of the IR spectrum is naturally of greater interest. A key difference with $P(\omega)$ is that the spectrum is not normalized and thus we cannot simply substitute $I(\omega)$ for $P(\omega)$ in Eq. 11. One approach is to use the unnormalized spectrum obtained as $I(\omega;T_b) = I(\omega;T_a)\, e^{-(\beta_b-\beta_a)\Delta U_{IR}(\omega)}$, the results of which are shown in Fig. 4a. The spectra predicted this way are in reasonable agreement with those calculated explicitly at the different temperatures. The key differences are, however, an issue of the overall intensity. This can be reasonably remedied by using the change in the frequency distribution normalization as a proxy, namely,

$$I_{pred}(\omega;T_b) = \frac{I(\omega;T_a)\, e^{-(\beta_b-\beta_a)\Delta U_{IR}(\omega)}}{\int P(\omega;T_a)\, e^{-(\beta_b-\beta_a)\Delta U(\omega)}\, d\omega}. \tag{12}$$

The results for this approach are presented in Fig. 4b. They are in excellent agreement with the explicit calculations of $I(\omega,T)$, with only slight differences for $T \geq 340$ K in the

width of the spectrum. As with $P(\omega)$, this renormalization provides a better description of the T-dependent spectra, but also results in an only approximate isosbestic point (Fig. 4b) rather than a precise one (Fig. 4a).

In summary, we have directly evaluated the temperature derivatives of the OH frequency distribution and IR spectrum of HOD in D_2O and shown how they can be used to predict the behavior over a wide range of temperatures (*e.g.*, 280-360 K) using a van't Hoff relation. The competition between Coulombic and Lennard-Jones interactions underlies the spectral properties, including the location of a (near) isosbestic point. A precise isosbestic point is not observed due to a subtle renormalization of the non-norm-conserving van't Hoff factor. The approaches described here should be useful in understanding and predicting the temperature dependence for a wide range of spectroscopic measurements probing liquids, including Raman and two-dimensional IR photon echo spectra.

Computational Methods

MD simulations of 343 TIP4P/2005[44] molecules in a periodic simulation cell of side length 21.725311 Å (ρ = 0.997 g/cm^3) were carried out using the Large-scale Atomic/Molecular Massively Parallel Simulator (LAMMPS).[45] A 1 fs timestep was used with the SHAKE algorithm to hold the water bonds and angle rigid (tolerance of 1×10^{-4}) and the electrostatics described with the Particle-Particle-Particle Mesh Ewald summation method[46,47] (tolerance of 1×10^{-4}). At 298.15 K, six 4 ns NVT trajectories were propagated with positions and energies saved every 4 fs; the IR spectra was calculated at 280, 320, 340, and 360 K from one 4 ns NVT trajectory at each temperature. Temperature was maintained with a Nosé-Hoover thermostat[48,49] with a damping parameter of 2 ps, long enough to avoid thermostat effects on the response functions $\phi(t)$ and $\phi_H(t)$. All reported uncertainties correspond to a 95% confidence interval according to the Student's t-distribution[50] over an average of six blocks (each block representing a 4 ns trajectory).

Acknowledgments

The authors thank Profs. Akihiro Morita and Damien Laage for useful comments. This work was supported by the National Science Foundation under Grant No. CHE-1800559. This material is based on the work supported by the National Science Foundation Graduate Research Fellowship under Grant Nos. 1540502 and 1451148. The calculations were performed at the University of Kansas Center for Research Computing.

References

(1) Pinkley, L. W.; Sethna, P. P.; Williams, D. Optical constants of water in the infrared: Influence of temperature. *J. Opt. Soc. Am.* **1977**, *67*, 494–499.

(2) Cunningham, K.; Lyons, P. A. Depolarization ratio studies on liquid water. *J. Chem. Phys.* **1973**, *59*, 2132–2139.

(3) Wyss, H. R.; Falk, M. Infrared spectrum of HDO in water and in NaCl solution. *Can. J. Chem.* **1970**, *48*, 607–614.

(4) Senior, W. A.; Verrall, R. E. Spectroscopic evidence for the mixture model in HOD solutions. *J. Phys. Chem.* **1969**, *73*, 4242–4249.

(5) Falk, M.; Ford, T. A. Infrared spectrum and structure of liquid water. *Can. J. Chem.* **1966**, *44*, 1699–1707.

(6) Hare, D. E.; Sorensen, C. M. Raman spectroscopic study of dilute HOD in liquid H_2O in the temperature range -31.5 to 160°C. *J. Chem. Phys.* **1990**, *93*, 6954–6961.

(7) Hare, D. E.; Sorensen, C. M. Raman spectroscopic study of bulk water supercooled to -33°C. *J. Chem. Phys.* **1990**, *93*, 25–33.

(8) Maréchal, Y. Infrared spectra of water. I. Effect of temperature and of H/D isotopic dilution. *J. Chem. Phys.* **1991**, *95*, 5565–5573.

(9) Libnau, F. O.; Toft, J.; Christy, A. A.; Kvalheim, O. M. Structure of liquid water determined from infrared temperature profiling and evolutionary curve resolution. *J. Am. Chem. Soc.* **1994**, *116*, 8311–8316.

(10) Libnau, F. O.; Kvalheim, O. M.; Christy, A. A.; Toft, J. Spectra of water in the near- and mid-infrared region. *Vib. Spectrosc.* **1994**, *7*, 243–254.

(11) Iwata, T.; Koshoubu, J.; Jin, C.; Okubu, Y. Temperature dependence of the mid-infrared OH spectral band in liquid water. *Appl Spectrosc* **1997**, *51*, 1269–1275.

(12) Walrafen, G. E.; Fisher, M. R.; Hokmabadi, M. S.; Yang, W. H. Temperature dependence of the low- and high-frequency Raman scattering from liquid water. *J. Chem. Phys.* **1986**, *85*, 6970–6982.

(13) Walrafen, G. E. Effects of equilibrium H-bond distance and angle changes on Raman intensities from water. *J. Chem. Phys.* **2004**, *120*, 4868–4876.

(14) Walrafen, G. E. Dispersion of the Raman depolarization ratio of HDO in water and heavy water from 295to368K, and from concentrated NaClO4/D2O/H2O. *J. Chem. Phys.* **2005**, *122*, 174502–9.

(15) Corcelli, S. A.; Skinner, J. L. Infrared and Raman line shapes of dilute HOD in liquid H_2O and D_2O from 10 to 90°C. *J. Phys. Chem. A* **2005**, *109*, 6154–6165.

(16) Smith, J.; Cappa, C.; Wilson, K.; Cohen, R.; Geissler, P.; Saykally, R. Unified description of temperature-dependent hydrogen-bond rearrangements in liquid water. *Proc. Natl. Acad. Sci.* **2005**, *102*, 14171–14174.

(17) Geissler, P. L. Temperature dependence of inhomogeneous broadening: On the meaning of isosbestic points. *J. Am. Chem. Soc.* **2005**, *127*, 14930–14935.

(18) Geissler, P. L. Water interfaces, solvation, and spectroscopy. *Annu. Rev. Phys. Chem.* **2013**, *64*, 317–337.

(19) Nicodemus, R. A.; Ramasesha, K.; Roberts, S. T.; Tokmakoff, A. Hydrogen bond rearrangements in water probed with temperature-dependent 2D IR. *J. Phys. Chem. Lett.* **2010**, *1*, 1068–1072.

(20) Nicodemus, R. A.; Corcelli, S. A.; Skinner, J. L.; Tokmakoff, A. Collective hydrogen bond reorganization in water studied with temperature-dependent ultrafast infrared spectroscopy. *J. Phys. Chem. B* **2011**, *115*, 5604–5616.

(21) Paesani, F. Temperature-Dependent Infrared Spectroscopy of Water from a First-Principles Approach. *J. Phys. Chem. A* **2011**, *115*, 6861–6871.

(22) Sakaguchi, S.; Ishiyama, T.; Morita, A. Theory and efficient computation of differential vibrational spectra. *J. Chem. Phys.* **2014**, *140*, 144109.

(23) Sakaguchi, S.; Ishiyama, T.; Morita, A. Theory and efficient computation of differential vibrational spectra (vol 140, 144109, 2014). *J. Chem. Phys.* **2014**, *141*, 149901.

(24) Joutsuka, T.; Morita, A. Efficient computation of difference vibrational spectra in isothermal–isobaric ensemble. *J. Phys. Chem. B* **2016**, *120*, 11229–11238.

(25) Joutsuka, T.; Morita, A. Improved theory of difference vibrational spectroscopy and application to water. *J. Chem. Theor. Comp.* **2016**, *12*, 5026–5036.

(26) Pattenaude, S. R.; Streacker, L. M.; Ben-Amotz, D. Temperature and polarization dependent Raman spectra of liquid H_2O and D_2O. *J Raman Spectrosc* **2018**, *49*, 1860–1866.

(27) Morawietz, T.; Marsalek, O.; Pattenaude, S. R.; Streacker, L. M.; Ben-Amotz, D.; Markland, T. E. The interplay of structure and dynamics in the raman spectrum of liquid water over the full frequency and temperature range. *J. Phys. Chem. Lett.* **2018**, *9*, 851–857.

(28) Dellago, C.; Bolhuis, P. G. Activation energies from transition path sampling simulations. *Mol. Simul.* **2004**, *30*, 795–799.

(29) Mesele, O. O.; Thompson, W. H. Removing the barrier to the calculation of activation energies. *J. Chem. Phys.* **2016**, *145*, 134107.

(30) Piskulich, Z. A.; Mesele, O. O.; Thompson, W. H. Removing the barrier to the calculation of activation energies: Diffusion coefficients and reorientation times in liquid water. *J. Chem. Phys.* **2017**, *147*, 134103–6.

(31) Piskulich, Z. A.; Mesele, O. O.; Thompson, W. H. Activation energies and beyond. *J. Phys. Chem. A* **2019**, *123*, 7185–7194.

(32) Fecko, C. J.; Loparo, J. J.; Roberts, S. T.; Tokmakoff, A. Local hydrogen bonding dynamics and collective reorganization in water: Ultrafast infrared spectroscopy of HOD/D_2O. *J. Chem. Phys.* **2005**, *122*, 054506.

(33) Corcelli, S. A.; Lawrence, C. P.; Skinner, J. L. Combined electronic structure/molecular dynamics approach for ultrafast infrared spectroscopy of dilute HOD in liquid H_2O and D_2O. *J. Chem. Phys.* **2004**, *120*, 8107–8117.

(34) Gruenbaum, S. M.; Tainter, C. J.; Shi, L.; Ni, Y.; Skinner, J. L. Robustness of frequency, transition dipole, and coupling maps for water vibrational spectroscopy. *J. Chem. Theor. Comp.* **2013**, *9*, 3109–3117.

(35) Hestand, N. J.; Strong, S. E.; Shi, L.; Skinner, J. L. Mid-IR spectroscopy of supercritical water: From dilute gas to dense fluid. *J. Chem. Phys.* **2019**, *150*, 054505.

(36) Kubo, R.; Toda, M.; Hashitsume, N. *Statistical Physics II*; Springer-Verlag, New York, 1978.

(37) Piskulich, Z. A.; Thompson, W. H. On the temperature dependence of liquid structure. *J. Chem. Phys.* **2020**, *152*, 011102.

(38) Piskulich, Z. A.; Thompson, W. H. The dynamics of supercooled water can be predicted from room temperature simulations. *J. Chem. Phys.* **2020**, *152*, 074505.

(39) Piskulich, Z. A.; Laage, D.; Thompson, W. H. Activation energies and the extended jump model: How temperature affects reorientation and hydrogen-bond exchange dynamics in water. *J. Chem. Phys.* **2020**, *153*, 074110.

(40) Bosio, L.; Chen, S.-H.; Teixeira, J. Isochoric temperature differential of the X-ray structure factor and structural rearrangements in low-temperature heavy water. *Phys. Rev. A* **1983**, *27*, 1468–1475.

(41) Urquidi, J.; Singh, S.; Cho, C. H.; Robinson, G. W. Origin of temperature and pressure effects on the radial distribution function of water. *Phys. Rev. Lett.* **1999**, *83*, 2348–2350.

(42) Skinner, L. B.; Benmore, C. J.; Neuefeind, J. C.; Parise, J. B. The structure of water around the compressibility minimum. *J. Chem. Phys.* **2014**, *141*.

(43) Pathak, H.; Späh, A.; Kim, K. H.; Tsironi, I.; Mariedahl, D.; Blanco, M.; Huotari, S.; Honkimäki, V.; Nilsson, A. Intermediate range O–O correlations in supercooled water down to 235 K. *J. Chem. Phys.* **2019**, *150*, 224506.

(44) Abascal, J. L. F.; Vega, C. A general purpose model for the condensed phases of water: TIP4P/2005. *J. Chem. Phys.* **2005**, *123*, 234505.

(45) Plimpton, S. Fast parallel algorithms for short-range molecular dynamics. *J. Comput. Phys.* **1995**, *117*, 1–19.

(46) Darden, T.; York, D.; Pedersen, L. Particle mesh Ewald: An N·log(N) method for Ewald sums in large systems. *J. Chem. Phys.* **1993**, *98*, 10089–10092.

(47) Pollock, E. L.; Glosli, J. Comments on PPPM, FMM, and the Ewald method for large periodic Coulombic systems. *Comput. Phys. Comm.* **1995**, *95*, 93–110.

(48) Nose, S. A molecular dynamics method for simulations in the canonical ensemble. *Mol. Phys.* **1984**, *52*, 255–268.

(49) Hoover, W. G. Canonical dynamics: Equilibrium phase-space distributions. *Phys. Rev. A* **1985**, *31*, 1695–1697.

(50) Shoemaker, D. P.; Garland, C. W.; Nibler, J. W. *Experiments in Physical Chemistry*; McGraw-Hill: New York, 1989.